Analytical approach to Coulomb focusing in strong-field ionization. I. Nondipole effects

Jiří Daněk,* Karen Z. Hatsagortsyan,† and Christoph H. Keitel
Max-Planck-Institut für Kernphysik, Saupfercheckweg 1, 69117 Heidelberg, Germany

(Received 27 March 2018; published 13 June 2018)

The role of the Coulomb potential of the atomic core for the creation of caustics in the photoelectron momentum distribution for tunneling ionization in a linearly polarized strong laser field, commonly termed Coulomb focusing, is investigated within classical theory beyond the dipole approximation. Coulomb focusing is addressed by analytical calculation of Coulomb momentum transfer to the tunneled electron due to rescatterings, while applying perturbation theory and classifying the recollisions either as fast or as slow. With the help of the derived analytical treatment, we analyze the origin of the counterintuitive energy-dependent bend of the Coulomb focusing cusp in the photoelectron momentum distribution in a linearly polarized laser field in the nondipole regime, and its scaling with the field parameters. The high-order recollisions are shown to be responsible for a decrease of the bend of the cusp at very low energies in this regime.

DOI: 10.1103/PhysRevA.97.063409

I. INTRODUCTION

Since the seminal works of Perelomov, Popov, and Terent'ev (PPT) [1–6], it has been known that the ionization rate of the atom in a strong laser field can be significantly disturbed by the Coulomb field of the atomic core. Later it was realized that the Coulomb field of the atomic core imprints specific signatures on the momentum distribution of photoelectrons [7], which arise during electron excursion in the laser field after the release (tunneling) from the bound state. The Coulomb field effect on the electron dynamics is conspicuous, first of all near the tunnel exit [8], and further during rescatterings [9]. While the first effect exists at any polarization of the laser field, the rescattering is mostly efficient in the case of linear polarization, although even in a laser field of elliptical polarization, rescattering and consequent Coulomb effects can take place [10–18].

Hard rescatterings with a small impact parameter induce well-known processes of above-threshold ionization [19], high-order-harmonic generation [20,21], and nonsequential double ionization [22]. In contrast to that, due to multiple forward scattering of ionized electrons by the atomic core at large impact parameters during oscillation in the laser field, the electrons with large transverse momentum at the ionization tunnel exit finally appear with low transverse momentum. Accordingly, the large initial transverse momentum space at the tunnel exit is squeezed into the asymptotic small one, i.e., the Coulomb field focuses electrons in the momentum space along the laser polarization direction, which is termed Coulomb focusing [7,23,24]. In early experiments, the traces of Coulomb focusing was observed as cusps and humps in the photoelectron momentum distribution [25–28]. Recently, due to advancements of the midinfrared laser technique [29], the interest in Coulomb focusing has been significantly increased with observation of rich structures in the photoelectron momentum distribution near the ionization threshold in long-wavelength laser fields, the so-called low-energy structures (LES) [30–32], very-low-energy structures [33,34], and zero-energy structures [35–40]. The origin of LES has been traced to multiple forward scattering by the Coulomb field, which induces transverse and longitudinal bunching of the electron momentum space [41–49]. LES are well resolved in midinfrared laser fields, when the Keldysh parameter is small, the interaction is essentially in the tunneling regime, and classical features of the three-step model [9] are evident.

For nonperturbative quantum descriptions of Coulomb field effects, different modifications of the strong-field approximation (SFA) [50–52] have been developed [53–60]. The Coulomb-corrected SFA of [53,54], which employs the quasiclassical electron wave function in the continuum in laser and Coulomb fields, has been successfully applied for the explanation of LES [43]. A similar but more systematic R-matrix theory [55–57] has also been extended to treat recollisions [61,62]. It appears that the perturbative SFA is also able to account for LES [63–67] when appropriate trajectories with soft recollisions [46] are included. However, this description is only qualitative because for a correct quantitative description, the effect of multiple recollisions should be taken into account.

In midinfrared laser fields, the electron dynamics after tunneling is mainly classical because the characteristic energies of the process, namely, the ionization and ponderomotive potentials, greatly exceed the photon energy in this regime. Therefore, the classical trajectory Monte Carlo (CTMC) method [68–70] has been successful in explaining LES features; see, e.g., [32,42,47,71,72]. Although both Coulomb-corrected SFA and CTMC successfully predict the existence of LES, they deliver only a little insight into the underlying physics as they both employ classical trajectories via numerical calculations which hide the physical picture of the transformation of the electron's initial momentum space at the tunnel exit into the asymptotic one at the detector.

Coulomb focusing arises due to the long-range Coulomb interaction between the tunnelled electron and its parent ion. This interaction is conspicuous at rescattering points when the

*danek@mpi-hd.mpg.de
†k.hatsagortsyan@mpi-hd.mpg.de

 ©2018 American Physical Society

tunneled electron revisits the atomic core during its excursion driven by the laser field. Usually the momentum transfer during high-order rescattering events is decreasing with its order. However, the decrease is not monotonous and the accurate description requires accounting also for high-order rescatterings [45,71]. The understanding of Coulomb focusing requires quantitative information on the Coulomb momentum transfer (CMT) at effective recollisions. For instance, the essential point in the LES explanation was establishing the fact of the nonuniform dependence of CMT at recollisions with respect to the ionization phase (laser field phase at the ionization moment) and the reason for that.

Moreover, recent experiments [18,73] have shown that Coulomb focusing is significantly modified in the nondipole regime. The breakdown of the dipole approximation was first observed in the case of linear polarization of the laser field [73] as a counterintuitive shift of the photoelectron momentum distribution peak opposite to the laser propagation direction, which was attributed to the interaction of the tunneled electron with the Coulomb field of the parent ion. Further numerical calculations of the time-dependent Schrödinger equation have shown that the photoelectron momentum distribution shift with respect to the dipole approximation case is not uniform, but momentum dependent [74]. The same conclusion has been drawn from the classical [75] and Coulomb-corrected SFA [76] calculations. However, the intuitive explanation of the nondipole features of photoelectron momentum distribution is still missing.

In this paper, we develop a classical analytical theory for the description of Coulomb focusing with respect to the underlying momentum transfer due to the Coulomb interaction. We derive analytical formulas for the CMT to the recolliding electron at multiple recollisions, while classifying the recollisions as either fast or slow recollision. We include nondipole effects, accounting for the laser magnetic-field-induced drift of the ionized electron along the laser propagation direction during the excursion in the laser field. The Coulomb field of the atomic core is treated as a perturbation to the laser-driven trajectory near the recollision point. The scaling of the CMT at the recollision (rec-CMT) with respect to the rescattering parameters (momentum and impact parameter) is derived. We also address the CMT taking place at the initial part of the trajectory, where the electron starts at the tunnel exit and recedes from the atom. Our inquiry leads to high-order corrections to the known formula for the initial CMT (in-CMT), which are necessary for keeping the overall precision of our model. In our approach, CMT is a perturbation with respect to the instantaneous electron momentum at the rescattering (at the tunnel exit); however, it may have a nonperturbative contribution with respect to the electron final momentum. We employ our framework for investigation of the counterintuitive energy-dependent bend of the cusp in the photoelectron momentum distribution, revealing a fine interplay of the nondipole and Coulomb field effects. We find a direct relationship of multiple recollisions and the fine structure of the cusp.

The structure of the paper is the following. In Sec. II, the model of Coulomb focusing is introduced. The transverse and longitudinal rec-CMT are calculated in all generality in Sec. III. In Sec. IV, we derive the revised formula for in-CMT. The nondipole effects in Coulomb focusing are investigated in Sec. V. The conclusion is given in Sec. VI.

II. THE MODEL

We consider the tunneling ionization regime of an atom in a strong laser field when the Keldysh parameter is small [50], i.e., $\gamma \equiv \sqrt{I_p/2U_p} \ll 1$, with the ionization potential I_p and the ponderomotive potential $U_p = E_0^2/4\omega^2$. Atomic units are used throughout, unless mentioned otherwise. The laser field is linearly polarized,

$$\begin{aligned} \mathbf{E}(u) &= E_0 \mathbf{e} \cos u, \\ \mathbf{B}(u) &= \mathbf{n} \times \mathbf{E}(u), \end{aligned} \tag{1}$$

where $u = \omega(t - z/c)$ is the laser phase, $\mathbf{B}(u)$ is the laser magnetic field, E_0 and ω are the amplitude and the angular frequency of the laser field, respectively, c is the speed of light, and $\mathbf{e} = (1,0,0)$ and $\mathbf{n} = (0,0,1)$ are the unit vectors along the laser polarization and propagation directions, respectively. We assume that the electron has tunneled out from the atomic bound state, which is described by the PPT ionization rate. The latter provides the probability for the initial transverse momentum distribution [4],

$$w(p_\perp) \propto \exp\left(-\frac{p_\perp^2}{\Delta_\perp^2}\right), \tag{2}$$

where $\Delta_\perp = E_0^{1/2}/(2I_p)^{1/4}$. The initial longitudinal momentum with respect to the laser field direction at the ionization moment t_i is assumed to be vanishing, and the initial coordinate is at the tunnel exit.

We consider the nondipole regime of interaction and will keep for the solution of the equations of motion the leading terms with respect to $1/c$, which describe the laser magnetic-field-induced drift of the electron in the laser propagation direction. The physical condition of the applied $1/c$ expansion is the smallness of the laser-induced drift distance during the laser period $d \sim \lambda\xi^2/2$ [77] with respect to the recollision impact parameter $\rho \sim 2\pi p_\perp/\omega$: $d \ll \rho$, where $\xi = E_0/(c\omega)$ is the invariant laser field parameter, λ is the laser wavelength, $p_\perp = \sqrt{p_y^2 + p_z^2}$ is the electron transverse momentum, $p_\perp \sim 2\Delta_\perp = 2\kappa\sqrt{E_0/E_a}$, $\kappa = \sqrt{2I_p}$ is the atomic momentum, I_p is the ionization potential, and $E_a = \kappa^3$ is the atomic field. Note that the introduced small parameter $\epsilon \equiv d/\rho$, in fact, is directly related to the Lorentz deflection parameter [78,79],

$$\Gamma_R = \epsilon^2 = \frac{\kappa c \xi^3}{16\omega}. \tag{3}$$

The magnetically induced drift changes the impact parameter of recollisions and, in this way, modifies Coulomb focusing. However, we stress that during the brief recollision time δt, the effect of the magnetically induced drift is negligible because the change of the impact parameter due the drift during the recollision time, which can be estimated as $\delta\rho \sim (\lambda\xi^2)(\omega\delta t)$, is much smaller than the impact parameter itself. In fact, we estimate the recollision time as $\delta t \sim \rho/v_\parallel$, with the electron longitudinal velocity at the recollision $v_\parallel \sim E_0/\omega$, and the ratio $\delta\rho/\rho \sim \epsilon\gamma\sqrt{E_0/E_a}$. We consider the tunneling regime when the Keldysh parameter is small $\gamma \ll 1$ and the field is small

to hinder the over-the-barrier ionization, i.e., $E_0/E_a \ll 1$. The latter means that $\delta\rho/\rho$, i.e., the change of the impact parameter due the drift during the recollision time, has an additional smallness in addition to the small parameter ϵ and, consequently, can be neglected in our discussion.

Our aim is to find an analytical expression for CMT. We assume that the Coulomb field effect is not negligible only near recollision points and near the tunnel exit, where it is treated as a perturbation with respect to the laser field. The latter assumptions are valid, first, if the Coulomb force is smaller with respect to the laser field at the recollision point and at the tunnel exit, $Z/r_r^2, Z/x_e^2 \ll E_0$, with the charge of the atomic core Z, and the recollision and tunnel exit coordinates $r_r \sim \Delta_\perp/\omega$ and $x_e \sim I_p/E_0$, respectively, and, second, if the quiver amplitude of the electron in the laser field greatly exceeds the recollision and the tunnel exit coordinates $E_0/\omega^2 \gg r_r, x_e$. The first pair of these conditions reads

$$\frac{Z}{\kappa}\gamma^2 \ll 1, \tag{4}$$

$$\frac{Z}{\kappa}\frac{E_0}{E_a} \ll 1, \tag{5}$$

and the second pair gives

$$\gamma\sqrt{\frac{E_0}{E_a}} \ll 1, \tag{6}$$

$$\gamma^2 \ll 1. \tag{7}$$

These conditions are well fulfilled in the tunneling regime.

The tunneled electron dynamics in the continuum after tunneling is governed by Newton equations,

$$\frac{d\mathbf{p}}{dt} = -\mathbf{E} - \frac{\mathbf{v}}{c}\times\mathbf{B} - \frac{Z\mathbf{r}}{r^3}, \tag{8}$$

where $\mathbf{v}$ is the electron velocity. The Coulomb field of the atomic core will be treated by perturbation theory during the recollision and we expand the momentum and coordinate as

$$\begin{aligned}\mathbf{p} &= \mathbf{p}_0 + \mathbf{p}_1 + \cdots,\\ \mathbf{r} &= \mathbf{r}_0 + \mathbf{r}_1 + \cdots.\end{aligned} \tag{9}$$

The unperturbed trajectory $\mathbf{r}_0(u)$ is determined by the laser field,

$$\frac{d\mathbf{p}_0}{dt} = -\mathbf{E}\Big(1 - \frac{\mathbf{n}\cdot\mathbf{v}_0}{c}\Big) - \mathbf{n}\frac{\mathbf{v}_0\cdot\mathbf{E}}{c}, \tag{10}$$

and momentum transfer due to the Coulomb field at the recollision is described by the trajectory in the first order of perturbation,

$$\frac{d\mathbf{p}_1}{dt} = -\frac{Z\mathbf{r}_0}{r_0^3}, \tag{11}$$

with $r_0 = |\mathbf{r}_0|$. Taking into account that $du/dt = \omega(t - v_z/c)$, and the integral of motion in a plane laser field $\Lambda_0 \equiv \varepsilon_0(u) - cp_{0z}(u) = \text{const}$, with the electron energy ε_0, Eq. (10) is integrated, providing the laser-driven momentum evolution,

$$\begin{aligned}p_{0x}(u) &= p_{xr} + [A_x(u) - A_x(u_r)],\\ p_{0y}(u) &= p_{yr},\\ p_{0z}(u) &= p_{zr} + p_{zd}(u,u_r),\end{aligned} \tag{12}$$

with the laser vector potential $A_x(u) = -(E_0/\omega)\sin u$. The initial conditions are defined at the recollision point with the recollision phase u_r and the recollision momentum $\mathbf{p}_r = (p_{xr}, p_{yr}, p_{zr})$, aiming at application of the solution near the recollision point. Here, the drift momentum induced by the laser magnetic field is

$$p_{zd}(u,u_r) \equiv \frac{p_{xr}}{c}[A_x(u) - A_x(u_r)] + \frac{1}{2c}[A_x(u) - A_x(u_r)]^2, \tag{13}$$

where the integral of motion is approximated, $\Lambda_0 \approx c^2$, to keep the leading term in the $1/c$ expansion. The unperturbed electron trajectory near the recollision point is

$$\begin{aligned}x_0(u) &= \frac{E_0}{\omega^2}[\cos u - \cos u_r + (u - u_r)\sin u_r]\\ &\quad + \frac{p_{xr}}{\omega}(u - u_r) + x_r,\\ y_0(u) &= \frac{p_{yr}}{\omega}(u - u_r) + y_r,\\ z_0(u) &= \frac{p_{zr}}{\omega}(u - u_r) + z_d(u) + z_r,\end{aligned} \tag{14}$$

with the recollision coordinate $\mathbf{r}_r = (x_r, y_r, z_r)$, and the laser magnetically induced drift coordinate

$$z_d(u) = \int_{u_r}^{u} p_{zd}(u', u_r)du'. \tag{15}$$

Once the zero-order equations are solved, the momentum transfer due to the Coulomb field at the recollision can be derived as the first-order correction,

$$\mathbf{p}_1 = -\frac{Z}{\omega}\int_{u_r-\delta}^{u_r+\delta}\frac{\mathbf{r}_0(u')}{r_0^3(u')}du', \tag{16}$$

where $\mathbf{r}_0(u) = [x_0(u), y_0(u), z_0(u)]$. The value of the parameter δ is coupled to the properties of the recollision and will be discussed in the next section.

In the discussion above, the Coulomb field effect is accounted for only near recollision points and near the tunnel exit, where it is treated as a perturbation with respect to the laser field. Still Eq. (16) for CMT includes nonperturbative Coulomb effects via dependence on the recollision parameters, i.e., the electron momentum $\mathbf{p}_r$ and coordinate $\mathbf{r}_r$ at the recollision point. In fact, the multiple recollisions preceding the currently discussed one can have a significant contribution to the considered $\mathbf{p}_r$ and $\mathbf{r}_r$, although the Coulomb field is perturbation at every single one of them.

III. MOMENTUM TRANSFER DURING RECOLLISIONS

A. Classification of recollisions

For estimation of rec-CMT, we first classify recolliding trajectories. There are two characteristic recolliding trajectories: (1) when the electron longitudinal velocity is vanishing at the recollision point, $x_r = 0$ and $p_{xr} = 0$, and (2) when the electron has the highest velocity at the recollision point, $x_r = 0$, $|\mathbf{p}_r| \neq 0$, and $\mathbf{E}(u_r) = 0$. We will call the above-mentioned two types of recollisions a slow recollision and a fast recollision, respectively; see Fig. 1. The first type of recollision corresponds to the peak of the momentum transfer

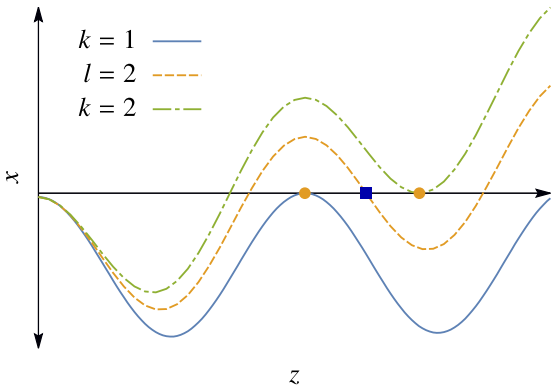

FIG. 1. Green (dot-dashed line) and blue (dashed line) trajectories correspond to slow recollision with $k = 1$ and $k = 2$ (yellow circles), respectively. Yellow trajectory corresponds to fast recollision with $l = 2$ (blue square).

in dependence on the initial ionization phase, and the second type corresponds to the plateau of the momentum transfer, as discussed in [45]. Let us remark that the slow recollision is also known in the literature as "soft recollision" [46].

The momentum transfer to the recolliding electron due to the Coulomb field of the atomic core at the kth recollision event is given by Eq. (16). As the main contribution to the integrals comes near the recollision points, we expand the trajectory near the recollision phase where rec-CMT takes place. We approximate the trajectory of the electron of Eq. (14) at the recollision point (x_r, y_r, z_r) with the recollision momentum (p_{xr}, p_{yr}, p_{zr}) near the recollision phase u_r as an expansion in $\sigma = u - u_r$, up to the σ^2 order,

$$\begin{aligned} x_0(u) &\approx x_r + \frac{p_{xr}}{\omega}\sigma - \frac{E(u_r)}{2\omega^2}\sigma^2, \\ y_0(u) &\approx y_r + \frac{p_{yr}}{\omega}\sigma, \\ z_0(u) &\approx z_r + \frac{p_{zr}}{\omega}\sigma - \frac{p_{xr}E(u_r)}{2c\omega^2}\sigma^2, \end{aligned} \tag{17}$$

because $z_d(u_r) = 0$ and $z_d'(u_r) = p_{zd}(u_r) = 0$.

B. Slow recollisions

In the case of slow recollision $p_{xr} = 0$, consequently, the trajectory in the leading order is

$$x_0(u) \approx x_r - \frac{E(u_r)}{2\omega^2}\sigma^2, \quad y_0(u) \approx y_r, \quad z_0(u) \approx z_r. \tag{18}$$

In the latter, we have neglected $p_\perp\sigma/\omega$ terms with respect to the recollision coordinate $\rho \sim p_\perp/\omega$ because the effective value of σ, derived from the condition $E_0\sigma^2/\omega^2 \sim \rho \sim p_\perp/\omega$, is $\sigma \sim \sqrt{p_\perp\omega/E_0} \sim \sqrt{\gamma}\sqrt{E_0/E_a} \ll 1$, and the transversal motion near the recollision point can be neglected for slow recollision. In general, the rescattering parameter x_r neither has to vanish at rescattering recollision nor has to be small. This assumption leads to generalization of the slow recollision for a larger class of recollisions with vanishing velocity.

From Eq. (16), we calculate rec-CMT for slow recollision along the trajectory approximated by Eqs. (18) while extending the integration limits to infinity ($\delta \to \infty$). The latter is well justified since large values of σ correspond to large deviation of the phase from the recollision point giving negligible contribution to the integration. The expression for rec-CMT at general slow recollisions with arbitrary x_r is given in Appendix A. In the case of common slow recollision $x_r \to 0$, we have the following simple formula for rec-CMT:

$$p_{1x,s}(u_r) \approx Z\frac{\mathrm{sign}\,[E(u_r)]}{3\sqrt{|E(u_r)|}}\frac{2^{3/2}\mathcal{P}_1}{r_r^{3/2}}, \tag{19}$$

$$p_{1y,s}(u_r) \approx -Z\frac{2^{3/2}\mathcal{P}_2 y_r}{\sqrt{|E(u_r)|}r_r^{5/2}}, \tag{20}$$

$$p_{1z,s}(u_r) \approx -Z\frac{2^{3/2}\mathcal{P}_2 z_r}{\sqrt{|E(u_r)|}r_r^{5/2}}, \tag{21}$$

where $r_r = \sqrt{x_r^2 + y_r^2 + z_r^2}$, $\mathcal{P}_1 = 3\pi P_{-1/2}^{-1}(0)/8 \approx 1.27$, and $\mathcal{P}_2 = 3\pi P_{-3/2}^{-1}(0)/8 \approx 0.927$, and $P_\nu^\mu(\eta)$ is the Legendre function of the first kind.

C. Fast recollisions

In the case of generalized fast recollision, we assume $x_r = 0$ and relax the condition on acceleration to $E(u_r) \approx 0$. In estimating rec-CMT, the electron trajectory near the recollision point in the leading order can be then approximated with

$$\begin{aligned} x_0(u) &\approx \frac{p_{xr}}{\omega}\sigma, \\ y_0(u) &\approx y_r + \frac{p_{yr}}{\omega}\sigma, \\ z_0(u) &\approx z_r + \frac{p_{zr}}{\omega}\sigma. \end{aligned} \tag{22}$$

With this approximation for the trajectory and tending the time integration limits to $\pm\infty$ (see Appendix B), we derive the following rec-CMT for fast recollision:

$$p_{1x,f} \approx \frac{2Zp_{\perp r}}{r_r p_{xr} p_r}, \tag{23}$$

$$p_{1y,f} \approx -\frac{2Zy_r}{r_r^2 p_r}, \tag{24}$$

$$p_{1z,f} \approx -\frac{2Zz_r}{r_r^2 p_r}, \tag{25}$$

where $p_{\perp r} = \sqrt{p_{yr}^2 + p_{zr}^2}$ and $p_r = \sqrt{p_{xr}^2 + p_{yr}^2 + p_{zr}^2}$.

Thus, we have derived analytical rec-CMT formulas for the common slow recollision ($x_r = 0$) given by Eqs. (19)–(21). In the general case of slow recollisions at nonvanishing x_r, the rec-CMT is determined by Eqs. (A1)–(A3) in Appendix A. For fast recollision, we have derived rec-CMT in Eqs. (23)–(25). When the recollision picture fails, the formulas of CMT are modified and given in Appendix B. The formulas for rec-CMT are expressed via parameters (coordinate and momentum) of the recollision and are valid even in the case when the global electron trajectory is significantly disturbed by the Coulomb field with respect to the laser-driven one. The nondipole effects in these formulas are accounted for in the parameters z_r and p_{zr}.

D. Simpleman estimations

The leading scaling of rec-CMT in Eqs. (19)–(21) and (23)–(25) can be explained from the following intuitive consideration. The transverse rec-CMT can be estimated as the transversal force $F_{\perp r} \sim 1/r_r^2$ acting during the recollision as

$$p_{1\perp} \sim F_{\perp r}\tau_r, \tag{26}$$

where τ_r is the duration of the recollision. We define the half of the recollision duration as a time when the electron longitudinal distance from the core reaches the value of the recollision distance, i.e., $x(\tau_r/2) = r_r$. In the case of slow recollision, $x(t) \approx -E(u_r)t^2/2$ and

$$\tau_{r,s} \sim 2\sqrt{2r_r/|E(u_r)|}, \tag{27}$$

while for fast recollision, $x_F(t) \approx p_{xr}t$ and

$$\tau_{r,f} \sim 2z_r/p_{xr}. \tag{28}$$

Thus, from Eqs. (26)–(28), we find estimations for the transverse rec-CMT,

$$p_{1\perp,s} \sim -\frac{2^{3/2}Z}{r_r^{3/2}\sqrt{|E(u_r)|}}, \tag{29}$$

$$p_{1\perp,f} \sim -\frac{2Z}{r_r p_{xr}}. \tag{30}$$

The longitudinal rec-CMT at slow recollision is easily estimated from the longitudinal force $F_{\parallel r} \sim -x_r(t)/z_r^3$ via

$$p_{1\parallel,s} \sim \int_{-\tau_{r,s}/2}^{\tau_{r,s}/2} F_{\parallel r}dt \sim -\frac{2Z}{r_r^3}\int_0^{\tau_{r,s}/2} x_s(t)dt = \frac{ZE(u_r)\tau_{r,s}^3}{2^3 3r_r^3},$$

which yields

$$p_{1\parallel,s} \sim \frac{2^{3/2}Z}{3\sqrt{|E(u_r)|}r_r^{3/2}}. \tag{31}$$

For estimation of the longitudinal rec-CMT at the fast recollision, one has to take into account that there is a compensation of rec-CMT stemming from trajectories before and after the recollision which can be incorporated by a reestablishment of the time dependence of $z_r(\tau) = z_r + p_{\perp r}\tau$ in $F_{\parallel r}$ and in the limit of $p_{xr} \gg p_{\perp r}$,

$$p_{1\parallel,f} \sim -Z\int_0^{\tau_{r,f}/2}\left[\frac{p_{xr}\tau}{(z_r + p_{\perp r}\tau)^3} - \frac{p_{xr}\tau}{(z_r - p_{\perp r}\tau)^3}\right]d\tau \approx \frac{Zp_{xr}p_{\perp r}\tau_{r,f}^3}{2^2 z_r^4}.$$

Once substituted from Eq. (28), we obtain the final formula

$$p_{1\parallel,f} \sim \frac{2Zp_{\perp r}}{z_r p_{xr}^2}. \tag{32}$$

Thus, by the applied simple estimations, the leading scaling of rec-CMT from Eqs. (23)–(25) is reproduced in the limit of $p_{\perp r} \ll p_{xr}$.

In this section, we have derived formulas for estimation of rec-CMT for specific recollision events, i.e., slow recollision and fast recollision. The rec-CMT for both of the recollisions can be represented in a unified form,

$$\mathbf{p}_1 \approx -\frac{Z\mathbf{r}_r}{r_r^3}\tau_r, \tag{33}$$

with an appropriate effective time of recollision τ_r that is different for slow recollision and fast recollision. We will employ this form for rec-CMT later in our analysis of nondipole effects. Before we approach the investigation of the nondipole effects, we need an estimate for in-CMT that is as accurate as the one we have for rec-CMT, which is derived in the next section.

IV. INITIAL COULOMB MOMENTUM TRANSFER

For the analytical estimation of in-CMT, we have to calculate the Coulomb momentum transfer to the electron, which takes place immediately after the leaving the tunnel exit, by using Eq. (16). The electron is at the tunnel exit x_i at ionization phase u_i with a transversal momentum $p_{\perp i}$ and is further accelerated by the laser field $E(u_i)$ in the longitudinal direction. We assume that the transversal motion is much smaller than the longitudinal one and expand the denominator of Eq. (16):

$$\frac{1}{[x^2(u) + y^2(u) + z^2(u)]^{3/2}} \approx \frac{1}{|x(u)|^3}\left[1 - \frac{3}{2}\frac{y^2(u) + z^2(u)}{x^2(u)}\right]. \tag{34}$$

Taking into account that $y = p_{yi}\sigma/\omega$ and $z = (p_{zi} + \overline{p}_{zd})\sigma/\omega$, the second term in the bracket can be estimated as

$$\frac{y^2(u) + z^2(u)}{x^2(u)} \sim \frac{p_{\perp i}^2\sigma^2}{\left(x_i - \frac{E_0}{2\omega^2}\sigma^2\right)^2\omega^2} + \frac{2p_{\perp i}\overline{p}_{zd}\sigma^2}{\left(x_i - \frac{E_0}{2\omega^2}\sigma^2\right)^2\omega^2}. \tag{35}$$

The first term in Eq. (35) is dominant over the second one by a factor of ϵ and, consequently, the second term is neglected. The order of magnitude of the first term is $\sim E_0/E_a \ll 1$, which justifies the expansion above. We estimated the effective region of $\sigma \equiv u - u_i$ from the relation $E_0\sigma^2/\omega^2 \sim x_i$.

The first-order approximation for in-CMT uses the unperturbed trajectory, which yields in-CMT formulas as derived in [80]; see Appendix C 1. Additionally, we calculate the second-order in-CMT with the first-order correction to the trajectory; see Appendix C 2. Combining the first- and second-order momentum corrections and expanding over the small parameter $1/(|E(u_i)|x_i^2) \sim E_0/E_a$, we arrive, in the quasistatic regime, with $x_i = -I_p/E(u_i)$, at the following expressions for the corrected in-CMT:

$$p_{2\parallel,\mathrm{in}} = \frac{Z\pi E(u_i)}{(2I_p)^{3/2}}\left[1 + \frac{2Z|E(u_i)|}{E_a\sqrt{2I_p}} - \frac{3p_{\perp i}^2}{8I_p} + O\left(\frac{E_0^2}{E_a^2}\right)\right], \tag{36}$$

$$p_{2\perp,\mathrm{in}} = -\frac{2Zp_{\perp i}|E(u_i)|}{(2I_p)^2} \times\left[1 + \frac{8Z|E(u_i)|}{3E_a\sqrt{2I_p}} - \frac{p_{\perp i}^2}{2I_p} + O\left(\frac{E_0^2}{E_a^2}\right)\right]. \tag{37}$$

For the analysis of the precision of the approximate formulas for CMT derived in Secs. III and IV, see Supplemental Material [81].

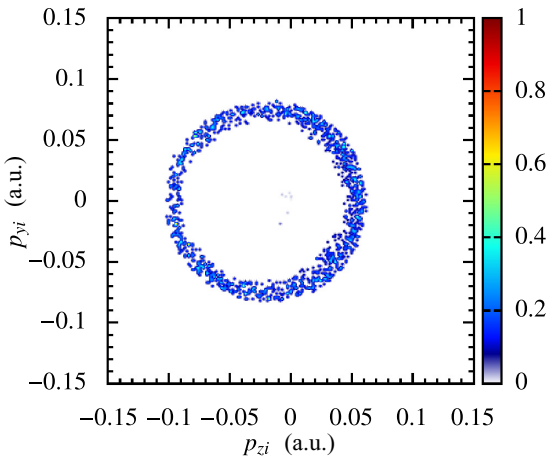

FIG. 2. Momentum space of the initial electron distribution at the tunnel exit, which contributes to the final momentum bin at $p_x = 0.588$ and $p_z = -0.0157$ a.u., corresponding to the first slow recollision. Note that the center of the ring is shifted to the negative-p_z direction.

V. NONDIPOLE EFFECTS

In this section, we demonstrate how the analytical formulas derived in the previous sections can be employed to gain insight into the process of Coulomb focusing in the nondipole regime. In particular, we provide an explanation for the observed counterintuitive and energy-dependent shift of the Coulomb focusing cusp in photoelectron momentum distribution [73]. This shift manifests a breakdown of the dipole approximation because in the dipole approximation, the cusp resides at the center of the photoelectron momentum distribution (i.e., $p_\perp = 0$).

Our aim is to investigate the origin of the shift and to explain its nontrivial shape in the nondipole regime. The central cusp is shifted along the laser propagation direction by a value varying with respect to the asymptotic longitudinal momentum, which can be seen in our CTMC simulation of photoelectron momentum distribution presented in Fig. 3.

For large longitudinal momenta, the shift is positive, which is expected, because of the positive drift momentum of the electron in the laser field along the propagation direction. Meanwhile, for lower longitudinal momenta, the shift becomes negative, but tends again to zero at very low longitudinal momenta. Such complex momentum dependence is intriguing and demands further investigation.

It is known that the electrons ending on the central cusp originate on a circle in the initial transverse momentum phase space at the ionization tunnel exit [18]. Moreover, the center of this circle gets shifted against the propagation direction in the nondipole regime as a compensation for the magnetically induced momentum drift, as shown in Fig. 2. The radius of this ring in the initial momentum space is an indicator of Coulomb focusing because it is equal to the total transverse rec-CMT for the cusp electrons. Using the formulas for rec-CMT given by Eq. (33), we will estimate the final transversal momenta of the cusp electrons at different final longitudinal momenta. Our aim is to deduce the reason for the behavior of the cusp momentum shift along the laser propagation direction from the analytical formula of the shift.

Let us follow an electron which originates at the tunnel exit with $p_{zi} \approx 0$ and $p_{yi} \neq 0$, and ends up at the cusp asymptotically (the laser wave propagates along the z axis and is polarized along the x axis). The advantage of this choice is that in the y direction, the dynamics is similar to the dipole case and the final y component of the electron momentum is vanishing,

$$p_{yf} = p_{yi} + p_{2y,\mathrm{in}} + p_{1y} \approx 0, \tag{38}$$

where p_{yi}, $p_{2y,\mathrm{in}}$, and p_{1y} are the y components of the electron initial momentum, in-CMT, and total rec-CMT, respectively. Moreover, from our analytical formulas, one can find a relationship between the y and z components of rec-CMT. The electron dynamics along the z axis is modified by the laser magnetic field. The final z component of the photoelectron momentum, according to Eq. (13), is

$$p_{zf} \approx p_{1z} + \frac{A^2(u_i)}{2c} - \frac{p_{xi}A(u_i)}{c}, \tag{39}$$

where p_{1z} is the rec-CMT for the discussed electron ionized at the laser phase u_i, and the laser wave propagates along the z axis and is polarized along the x axis. Assuming that the electron undergoes N rescatterings, Eq. (38) reads

$$p_{yi} + p_{2y,\mathrm{in}} + \sum_{n=1}^{N} p_{1y}^{(n)} \approx 0, \tag{40}$$

where $p_{1y}^{(n)}$ is the rec-CMT at the nth recollision.

Further, we exploit the possibility to estimate the individual rec-CMT as a product of the acting force during the recollision and the time of the recollision τ_n, as shown in Sec. III, Eq. (33),

$$p_{1y}^{(n)} \approx -\frac{Zy_n}{r_n^3}\tau_n. \tag{41}$$

Later we can apply the derived analytical formulas (19)–(21) and (23)–(25) to estimate recollision time τ_n precisely.

The change to the final momentum p_{1z} due to the Coulomb interaction is estimated as the sum of rec-CMTs, yielding

$$p_{1z} = \sum_{n=1}^{N} p_{1z}^{(n)} = -Z\sum_{n=1}^{N} \frac{z_n}{r_n^3}\tau_n. \tag{42}$$

As the recollision time τ_n and the recollision distance r_n are the same in Eqs. (40)–(42), we may use the former to simplify the expression for p_{1z}. For the latter, we need to estimate the recollision coordinates y_n and z_n. We define them stepwise from recollision to recollision as

$$\begin{aligned} y_1 &= (p_{yi} + p_{2y,\mathrm{in}})(t_1 - t_0), \\ y_2 &= (p_{yi} + p_{2y,\mathrm{in}})(t_2 - t_0) - Z\frac{y_1}{r_1^3}\tau_n(t_2 - t_1), \\ &\vdots \\ y_N &= (p_{yi} + p_{2y,\mathrm{in}})(t_N - t_0) - Z\sum_{n=1}^{N-1}\frac{y_n}{r_n^3}\tau_n(t_N - t_n), \end{aligned} \tag{43}$$

where t_0 is the ionization time, and t_n is the nth recollision time for $n \geqslant 1$. The upper formulas can be used to express Eq. (40) as follows:

$$p_{yi} + p_{2y,\mathrm{in}} = Z\sum_{n=1}^{N}\frac{\tau_n}{r_n^3}(p_{yi} + p_{2y,\mathrm{in}})(t_n - t_0) - Z^2\sum_{n=1}^{N}\frac{\tau_n}{r_n^3}\sum_{k=1}^{n-1}\frac{y_k}{r_k^3}\tau_k(t_n - t_k), \quad (44)$$

where the first term corresponds to first-order corrections to the zero-order trajectory and the second iterative term to the next-order corrections. When neglecting higher-order correction terms than the second order proportional to $\sim(\tau_n/r_n^3)^2$, we arrive after rearrangement at

$$Z\sum_{n=1}^{N}\frac{\tau_n}{r_n^3}(t_n - t_0) \approx 1 + Z^2\sum_{k<n}^{N}\frac{\tau_n\tau_k}{r_n^3 r_k^3}(t_n - t_k)(t_k - t_0). \quad (45)$$

The rescattering coordinate along the laser propagation direction z_r depends on the magnetically induced drift momentum of the electron ($p_{zi} = 0$ is chosen),

$$\begin{aligned} z_1 &= \overline{p}_{zd}^{(1)}(t_1 - t_0), \\ z_2 &= \overline{p}_{zd}^{(2)}(t_2 - t_0) - Z\frac{z_1}{r_1^3}\tau_n(t_2 - t_1), \\ &\vdots \\ z_N &= \overline{p}_{zd}^{(N)}(t_N - t_0) - Z\sum_{n=1}^{N-1}\frac{z_n}{r_n^3}\tau_n(t_N - t_n), \end{aligned} \quad (46)$$

where we used the magnetic drift from Eq. (13) (adjusted for the initial momentum p_{xi} along the polarization direction) to define the averaged drift momentum as

$$\overline{p}_{zd}^{(n)} \equiv \frac{1}{t_n - t_0}\int_{t_0}^{t_n}\left\{\frac{p_{xi}}{c}[A_x(t) - A_x(t_0)] + \frac{1}{2c}[A_x(t) - A_x(t_0)]^2\right\}dt. \quad (47)$$

Although in the tunneling regime $p_{xi} = 0$, we incorporate the in-CMT of Eq. (C10) into p_{xi} and set $p_{xi} = p_{2\parallel,\mathrm{in}}(u_i, p_{yi})$. When we substitute Eq. (46) into Eq. (42), we obtain

$$p_{1z} = -Z\sum_{n=1}^{N}\overline{p}_{zd}^{(n)}\frac{\tau_n}{r_n^3}(t_n - t_0) + Z^2\sum_{n=1}^{N}\frac{\tau_n}{r_n^3}\sum_{k=1}^{n-1}\frac{z_k}{r_k^3}\tau_k(t_n - t_k), \quad (48)$$

where the first term again corresponds to the first-order correction to the unperturbed trajectory and the second term corresponds to higher-order corrections. When neglecting the higher-order contributions $\sim(Z\tau_n/r_n^3)^2$ and employing the relationship of Eq. (45), we can write

$$p_{1z} \approx -\overline{p}_{zd}^{(1)} + Z\sum_{n=2}^{N}\left(\overline{p}_{zd}^{(1)} - \overline{p}_{zd}^{(n)}\right)\frac{\tau_n(t_n - t_0)}{r_n^3}. \quad (49)$$

The first term here describes rec-CMT at the first recollision and the other terms arise only due to the multiple recollisions.

In the case of a single recollision, the lengthy derivation above becomes very transparent,

$$p_{1z} = -Z\frac{z_1}{r_1^3}\tau_1 = -\frac{z_1}{y_1}p_{1y} = -\frac{z_1}{t_1 - t_0} = -\overline{p}_{zd}^{(1)}, \quad (50)$$

showing that in this case, the z component of rec-CMT equals the averaged (between the ionization and the rescattering time) drift momentum in the laser propagation direction.

One can give another intuitive perspective to Eq. (50) of the single recollision case while discussing the nondipole dynamics of the electron in the cusp, which has an initial momentum only along the laser propagation direction $\mathbf{p}_i = (0,0,p_{iz})$, and comparing it with the dipole case. The electron dynamics in the nondipole and in the dipole case will be similar if the recollision impact parameters are the same, $z_r = z_r^{(0)}$, where the parameters of the dipole case are indicated with the upper index $^{(0)}$. The rescattering coordinate in the nondipole case is $z_r = (p_{zi} + \overline{p}_{zd})(t_1 - t_0)$, while in the dipole case, it is simply $z_r^{(0)} = p_{zi}^{(0)}(t_1 - t_0)$. Thus, the electron dynamics will be similar in both cases if $p_{zi} = p_{zi}^{(0)} - \overline{p}_{zd}$, i.e., when the electron has an additional initial momentum opposite to the laser magnetically induced drift. The similar dynamics means, in particular, the same rec-CMT: $p_{1z} \approx p_{1z}^{(0)}$. Because in the nondipole case the cusp is at vanishing momentum, i.e., $p_{zi}^{(0)} + p_{1z}^{(0)} \approx 0$, we arrive at the relation $p_{1z} = -p_{zi} - \overline{p}_{zd}$, corresponding to Eq. (50) with $p_{zi} \approx 0$. The comparison links the averaged drift momentum before the first rescattering directly to the asymptotic momentum of the cusp electrons, which can now be estimated via Eq. (39) as

$$p_{zf} = p_{zi} + p_{1z} + \frac{A^2(u_i)}{2c} \approx -\overline{p}_{zd} + \frac{A^2(u_i)}{2c}, \quad (51)$$

where an intriguing interplay of the rec-CMT and of the magnetic drift contributions given by their opposite signs is revealed.

In the general case of multiple recollisions, we derive the asymptotic momentum using Eq. (49) as

$$p_{zf} \approx \frac{A^2(u_i)}{2c} - \frac{p_{xi}A(u_i)}{c} - \overline{p}_{zd}^{(1)} + Z\sum_{n=2}^{N}\left(\overline{p}_{zd}^{(1)} - \overline{p}_{zd}^{(n)}\right)\frac{\tau_n(t_n - t_0)}{r_n^3}, \quad (52)$$

where we sum over N recollisions. The first three terms in this equation can be combined, yielding

$$p_{zf} \approx -\overline{T}_{zd}^{(1)} + Z\sum_{n=2}^{N}\left(\overline{p}_{zd}^{(1)} - \overline{p}_{zd}^{(n)}\right)\frac{\tau_n(t_n - t_0)}{r_n^3}, \quad (53)$$

where

$$\overline{T}_{zd}^{(1)} \equiv \frac{1}{u_1 - u_0}\int_{u_0}^{u_1}\left[\frac{p_{xf}A(u)}{c} + \frac{A^2(u)}{2c}\right]du, \quad (54)$$

with $u_0 = u_i$ and asymptotic longitudinal momentum $p_{xf} \equiv -A(u_i) + p_{xi}$. Note that the latter equation coincides with Eq. (51) in the case of the single rescattering as $p_{zf} = -\overline{p}_{zd} + A^2(u_i)/(2c) = -\overline{T}_{zd}^{(1)}$.

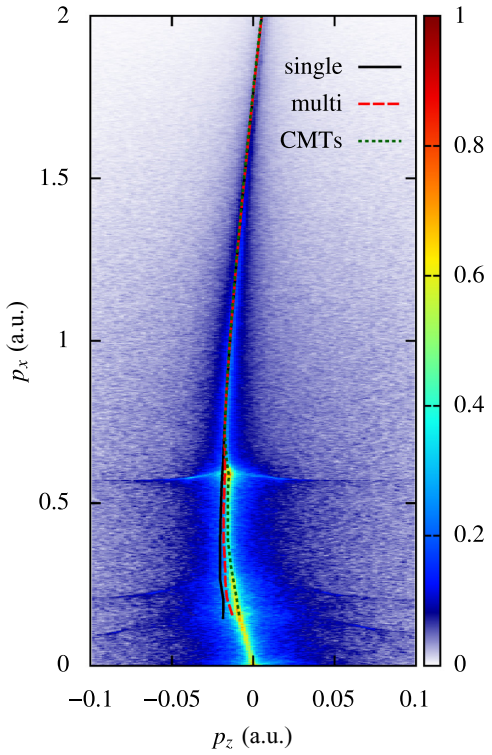

FIG. 3. The manifestation of the breakdown of the dipole approximation in photoelectron momentum distribution: CTMC simulation for hydrogen in intense laser pulse of linear polarization $E_0 = 0.0407$, $\omega = 0.012$ and the laser pulse duration $15.7/\omega$. The peak of the cusp was estimated via the first term in Eq. (53), $p_{zf} = -\overline{T}^{(1)}_{zd}$ (black solid line), further via the full Eq. (53) (red dashed line), and finally calculated as a sum of in-CMT and rec-CMT at each recollision via the analytical formulas of Sec. III (green dotted line).

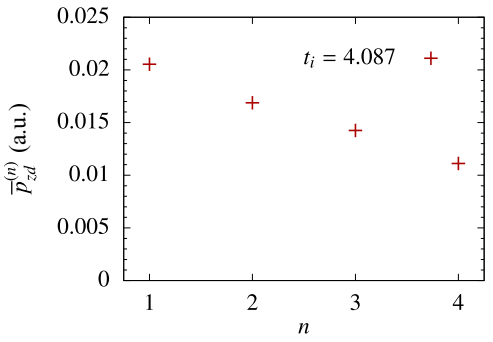

FIG. 4. The average magnetically induced drift momentum $\overline{p}^{(n)}_{zd}$ obtained until the nth rescattering for the ionization time $t_i = 4.087$, corresponding to the multiple rescattering case at $p_x \approx 0.3$.

Equation (53) is the main result of this section, which predicts the momentum shift of the Coulomb focusing cusp in the nondipole regime. In the case of a single recollision, which is the case at rather large final p_{xf} ($p_{xf} \gtrsim 0.52$ a.u. in Fig. 3), the momentum shift is determined by the first term $p_{zf} = -\overline{T}^{(1)}_{zd}$, i.e., by the average drift momentum due to the laser magnetic field $\overline{T}^{(1)}_{zd}$ during the electron excursion in the laser field. This term is determined only by the laser parameters as well as by the ionization and recollision phases, u_0 and u_1, respectively, via $\overline{T}^{(1)}_{zd}$; see also [75]. As we show in Fig. 3, our analytical formula $p_{zf} = -\overline{T}^{(1)}_{zd}$ represented by the solid line gives remarkable agreement with the cusp bend obtained by the fully numerical CTMC simulation for large and intermediate values of longitudinal momenta. It explains the positive shift of the cusp at large p_{xf}, as well as the counterintuitive negative shift at lower p_{xf} due to dominating rec-CMT at the single recollision.

In the case of more than one rescattering, the second term in Eq. (53) quantifies the role of multiple recollisions. Although the second term is more complicated for exact calculations, it contains a very simple qualitative message: the multiple recollisions are the reason to decrease the negative shift of the cusp and to move it towards the vanishing momenta at very low p_{xf}. The increasing number of recollisions at smaller p_{xf} leads to smaller negative shift of the cusp. This message stems from the fact that the second term is positive because of a relation $\overline{p}^{(k)}_{zd} > \overline{p}^{(l)}_{zd}$, at $k < l$; see Fig. 4.

Besides the mentioned qualitative message, Eq. (53) can also provide a way for a quantitative estimate of the nondipole momentum shift of the Coulomb focusing cusp. We compare the results derived from Eq. (53) with fully numerical CTMC simulations in Fig. 3. While the first-term contribution describes very well the peak of the cusp for large longitudinal momenta ($p_x \gtrsim 0.52$) when only a single rescattering exists (the horizontal fringes in the photoelectron momentum distribution correspond to the slow recollision condition; when one crosses the horizontal line towards lower longitudinal momenta, the number of rescatterings increases by one), a relatively large discrepancy appears at lower momenta, when the negative shift of the cusp begins to decrease, tending to zero at very low energies. The evaluation of the full Eq. (53) is shown in Fig. 3 by the dashed line. For the evaluation of the sum, the recollision coordinate and momentum are required for the specific trajectories ending up at the cusp. The latter are found approximately using the zero-order trajectory corrected by in-CMT. The initial momentum of the trajectories p_{yi} is found using the condition of Eq. (38), along with the analytical formulas for rec-CMT. The calculation via Eq. (53) shows the tendency to decrease the nondipole shift of the cusp at low energies. Thus, the simplified formula of Eq. (53) catches the main features of the cusp shift and proves the corresponding qualitative message.

In intuitive terms, when there is more than one rescattering, the nondipole dynamics is no longer similar to the dipole case. In fact, by a single parameter of the initial transverse momentum, one cannot fix the impact parameters of multiple scattering events to be the same as in the dipole case.

Whereas the positive offset of the bend can be attributed to the magnetic drift $p_{zd} = A^2(u_i)/2c$, the negative offset can be seen as a result of a counterbalance between the CMT p_{1z} and magnetically induced drift $p_{zd}(u,u_i)$. Due to the magnetically induced drift, the electron moves in the positive z-coordinate direction and gains a negative CMT in the z direction at the rescattering; the larger the drift (which is the case for the smaller longitudinal momentum), the larger the rec-CMT becomes in the z direction. Such picture holds for relatively large longitudinal momenta with a single recollision.

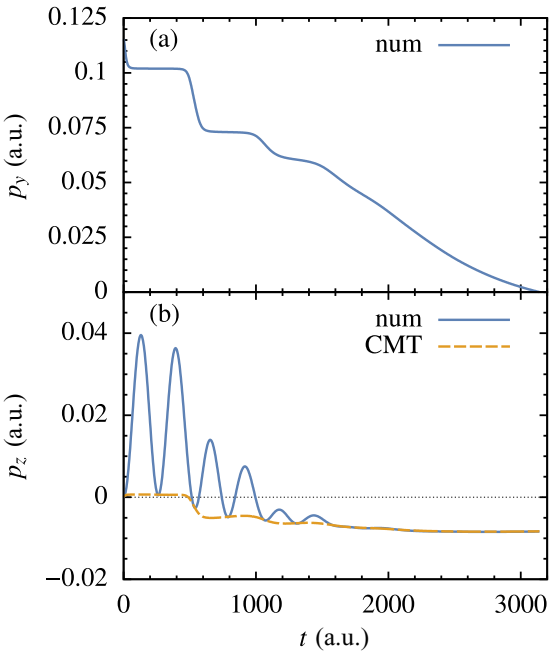

FIG. 5. The evolution of the compensated momentum of the electron $\mathbf{p}(t) + \mathbf{A}(t)$, which indicates the history of the CMT. The example shows the trajectory which ends up at the photoelectron momentum distribution cusp, tunneled at $t_i = -1.25$ with $p_{yi} = 0.116$ and $p_{zi} = 0$. (a) The p_y momentum component changes significantly at the end of the laser pulse ($t \approx 2200$). (b) Negative rec-CMT of the p_z at the end of the laser pulse where we isolated the contribution of the Coulomb interaction and plotted it by a yellow dashed line.

Nevertheless, the simulations have shown that the offset of the cusp at lower longitudinal momenta bends again towards the laser propagation direction, which is related to the increasing number of recollisions. The effective drift in this case is decreasing as $\overline{p}_{zd}^{(n)} < \overline{p}_{zd}^{(1)}$, which consequently decreases the total CMT in the z direction.

There is a second reason for the photoelectron momentum distribution cusp to shift towards vanishing momentum at very low energies. The low-energy electrons are still rather close to the parent ion when the interaction with the laser pulse is over. At this point and later on, the focusing property of the Coulomb field manifests and pulls these electrons towards the ion, decreasing further the transverse momentum; see an example in Fig. 5. As we can see in Fig. 5(a), the p_y momentum component changes significantly even at the end of the laser pulse, where the recollision picture no longer holds, and the condition given in Eq. (40) is not applicable. Figure 5(b) shows nontrivial negative CMT for the p_z at the tail of the laser pulse, which is not incorporated in our simplified discussion in this section. We estimated the position of the cusp by the asymptotic Kepler formula using the position from the numerical trajectory at the end of the laser pulse and the momenta from Eq. (53). The result is that only the low-energetic trajectories near the origin are slightly influenced, yielding a better agreement with the simulation in this region than shown in Fig. 3.

Finally, let us note that the dotted line in Fig. 3 shows the final momentum of the cusp electron, which is calculated using our analytical formulas for rec-CMT at individual rescatterings, with recollision parameters derived from the fully numerical trajectory. It serves as a proof of accuracy of the derived analytical formulas for rec-CMT.

VI. CONCLUSION

We have developed an analytical model for a quantitative description of Coulomb focusing effects in laser-induced strong-field ionization. Under the assumption that the Coulomb field effect is a perturbation for the near recollision laser-driven trajectory, we have derived analytical formulas for the CMT at recollisions which depend on the local recollision coordinate and momentum. For an effective treatment of CMT, we classify the recollisions into two types: slow and fast recollisions. The nondipole effects are shown to be negligible during the brief time of the recollision; however, they are indirectly incorporated in the theory via the recollision coordinate and momentum. Within the same model, we have derived essential higher-order corrections to the known expressions for the initial CMT at the tunnel exit [80] (the precision of the derived formulas is examined in the Supplemental Material [81]).

The applied perturbative treatment of the Coulomb field effect is well suited for the description of Coulomb focusing, which is due to multiple forward scattering of ionized electrons by the atomic core at large impact parameters during excursion in the laser field. In contrast, the hard rescatterings with a small impact parameter, which are not perturbative, induce well-known processes of above-threshold ionization.

The derived analytical formulas for the CMT, employed along with numerical simulations, can help one to gain insight into the detailed features of the Coulomb focusing effect in different laser field setups, e.g., in two-color or elliptically polarized laser fields. In particular, they allow estimation of the role of each particular rescattering event, which is hidden in the fully numerical CTMC simulation, but essentially helps to develop an intuitive picture for Coulomb focusing. The way in which the high-order rescatterings influence Coulomb focusing will be investigated in more detail in the second paper of this series.

Finally, we have employed the derived analytical formulas for CMT to gain insight into the nontrivial features of the photoelectron momentum distribution in the nondipole regime. We have obtained a simple analytical formula (53) describing the nondipole shift of the photoelectron momentum distribution cusp in the laser propagation direction. The peak of the cusp in the photoelectron momentum distribution in the nondipole regime is positive at large longitudinal momenta, but becomes negative at intermediate values, and moves again towards the laser propagation direction for even lower rates. We have explained this counterintuitive behavior of the peak of the cusp by relating it to the laser magnetically induced average drift. The increase of the negative shift of the cusp at decreasing longitudinal momentum is explained by the increase of the laser magnetically induced average drift until the single recollision. The decrease of the negative shift of the cusp at very low longitudinal momenta is shown to arise due to multiple rescatterings.

APPENDIX A: CMT AT SLOW RECOLLISIONS

From Eq. (16), we calculate rec-CMT for slow recollision along the trajectory approximated by Eqs. (18) while extending the integration limits to infinity ($\delta \to \infty$). The results yield

$$p_{1x,s} = \frac{-\pi Z}{\sqrt{2^3|E(u_r)|\left(y_r^2+z_r^2\right)r_r}}\left(\frac{3x_r}{r_r}P^{-1}_{-\frac{3}{2}}\left\{-\operatorname{sign}[E(u_r)]\frac{x_r}{r_r}\right\}\right.$$
$$\left. - \operatorname{sign}[E(u_r)]\ P^{-1}_{-\frac{1}{2}}\left\{-\operatorname{sign}[E(u_r)]\frac{x_r}{r_r}\right\}\right), \tag{A1}$$

$$p_{1y,s} = -\frac{3\pi Z y_r}{\sqrt{2^3|E(u_r)|\left(y_r^2+z_r^2\right)r_r^3}}\ P^{-1}_{-\frac{3}{2}}\left\{-\operatorname{sign}[E(u_r)]\frac{x_r}{r_r}\right\}, \tag{A2}$$

$$p_{1z,s} = -\frac{3\pi Z z_r}{\sqrt{2^3|E(u_r)|\left(y_r^2+z_r^2\right)r_r^3}}\ P^{-1}_{-\frac{3}{2}}\left\{-\operatorname{sign}[E(u_r)]\frac{x_r}{r_r}\right\}, \tag{A3}$$

where $r_r = \sqrt{x_r^2+y_r^2+z_r^2}$ and $P_\nu^\mu(\eta)$ is the Legendre function of the first kind which emerges during the integration, using the tabular integral [82]

$$\int_0^\infty \frac{x^{\mu-1}dx}{(1+2x\cos t+x^2)^\nu} = \left(\frac{2}{|\sin t|}\right)^{\nu-1/2}\Gamma\left(\nu+\frac{1}{2}\right)B(\mu,2\nu-\mu)P^{1/2-\nu}_{\mu-\nu-1/2}(\cos t), \tag{A4}$$

where $\Gamma(x)$ stands for the Gamma function, $B(x,y)$ for the Beta function, $P_\nu^\mu(x)$ for the Legendre function of the first kind, and $-\pi < t < \pi$, $0 < \mathrm{Re}(\mu) < \mathrm{Re}(2\nu)$.

For illustration, we show the behavior of the Legendre functions in Fig. 6. Both functions diverge for $\eta \to -1$, which is, however, out of the region of our interest since the condition $x_r \lesssim \sqrt{y_r^2+z_r^2}$ is fulfilled at the recollision and leads to the restriction on the argument of the Legendre function $|\operatorname{sign}[E(u_r)]\frac{x_r}{r_r}| \lesssim \frac{1}{\sqrt{2}}$. The other possible case of $x_r \gg \sqrt{y_r^2+z_r^2}$ along with $E(u_r)x_r > 0$ does not belong to the soft-recollision case. It corresponds to the hard-recollision case with a large rec-CMT, which is beyond the present treatment.

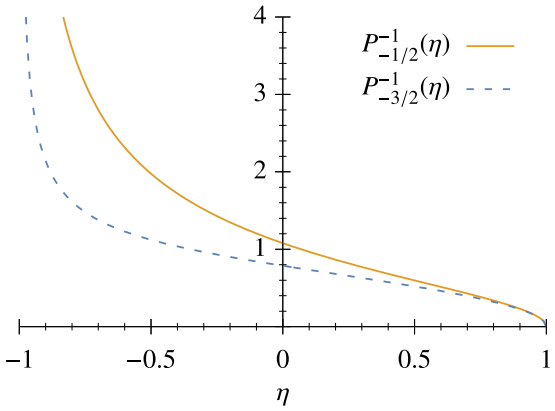

FIG. 6. The Legendre functions within the valid range given by Eqs. (A1)–(A3). Distinct values are $P^{-1}_{-3/2}(0) \approx 0.787$ and $P^{-1}_{-1/2}(0) \approx 1.08$. Both functions diverge at $\eta \to -1$, which is out of the region of our interest since physically relevant cases correspond to $|\eta| < 1/\sqrt{2}$.

The Legendre function of the first kind can be expressed for real $x \in [-1,1]$ as

$$P_\nu^\mu(x) = \frac{1}{\Gamma(1-\mu)}\left(\frac{1+x}{1-x}\right)^{\frac{\mu}{2}} \times {}_2F_1\left(-\nu,\nu+1;1-\mu;\frac{1-x}{2}\right), \tag{A5}$$

via the hypergeometric function ${}_2F_1(a,b;c;z)$ [82], which gives

$$P^{-1}_{-\frac{3}{2}}(0) = {}_2F_1\left(\tfrac{3}{2},-\tfrac{1}{2};2;\tfrac{1}{2}\right) = 0.786\,894, \tag{A6}$$

$$P^{-1}_{-\frac{1}{2}}(0) = {}_2F_1\left(\tfrac{1}{2},\tfrac{1}{2};2;\tfrac{1}{2}\right) = 1.078\,71. \tag{A7}$$

APPENDIX B: CMT AT FAST RECOLLISIONS

In the case of a fast recollision, the first-order correction to the momentum is given by Eq. (16), using the approximate expression for the trajectory of Eqs. (22). Once we substitute for the lower and upper limit of integration $u_r - \delta \to u_r + \sigma_1$ and $u_r + \delta \to u_r + \sigma_2$, respectively, we can evaluate the integrals for each component and arrive at

$$p_{1x,f} \approx Z\left\{\frac{p_{xr}[(y_r p_{yr}+z_r p_{zr})\sigma+\omega r_r]}{\left[p_{xr}^2 r_r^2+(y_r p_{zr}-z_r p_{yr})^2\right]\sqrt{p_{xr}^2\sigma^2+(p_{yr}\sigma+\omega y_r)^2+(p_{zr}\sigma+\omega z_r)^2}}\right\}_{\sigma_1}^{\sigma_2}, \tag{B1}$$

$$p_{1y,f} \approx Z\left\{\frac{-y_r p_{xr}^2\sigma-(y_r p_{zr}-z_r p_{yr})(\omega z_r+p_{zr}\sigma)}{\left[p_{xr}^2 r_r^2+(y_r p_{zr}-z_r p_{yr})^2\right]\sqrt{p_{xr}^2\sigma^2+(p_{yr}\sigma+\omega y_r)^2+(p_{zr}\sigma+\omega z_r)^2}}\right\}_{\sigma_1}^{\sigma_2}, \tag{B2}$$

$$p_{1z,f} \approx Z\left\{\frac{-z_r p_{xr}^2\sigma-(y_r p_{zr}-z_r p_{yr})(\omega y_r+p_{yr}\sigma)}{\left[p_{xr}^2 r_r^2+(y_r p_{zr}-z_r p_{yr})^2\right]\sqrt{p_{xr}^2\sigma^2+(p_{yr}\sigma+\omega y_r)^2+(p_{zr}\sigma+\omega z_r)^2}}\right\}_{\sigma_1}^{\sigma_2}. \tag{B3}$$

While in the dipole limit relation $y_r p_{zr} = z_r p_{yr}$ holds due to symmetry, in the nondipole case $y_r p_{zr} - z_r p_{yr} \approx y_r[p_{zd}(u_r,u_i) - \frac{1}{u_r-u_i}\int_{u_i}^{u_r} p_{zd}(u,u_i)du] \sim y_r\, c\xi^2$. The terms proportional to $(y_r p_{zr} - z_r p_{yr})^2$ in the denominators in Eqs. (B1)–(B3) are ξ^2 times smaller with respect to the leading term (in estimation we use $p_{xr} \sim c\xi$) and can therefore be neglected with respect to the expansion parameter ϵ of Eq. (3), which can be rewritten as $\epsilon \sim (\xi/\gamma)\sqrt{E_a/E_0}$. Using $p_{xr}\sigma/\omega \sim y_r$, one can show negligible contributions of the magnetic drift terms with respect to the leading one in the numerators of Eqs. (B2) and (B3) by a factor of ξ.

Thus, after neglecting the discussed terms, we have

$$p_{1x,f} \approx Z\left[\frac{p_{\perp r}\sigma+\omega}{p_{xr}r_r\sqrt{p_{xr}^2\sigma^2+(p_{yr}\sigma+\omega y_r)^2+(p_{zr}\sigma+\omega z_r)^2}}\right]_{\sigma_1}^{\sigma_2}, \tag{B4}$$

$$p_{1y,f} \approx Z\left[\frac{-\sigma y_r}{r_r^2\sqrt{p_{xr}^2\sigma^2+(p_{yr}\sigma+\omega y_r)^2+(p_{zr}\sigma+\omega z_r)^2}}\right]_{\sigma_1}^{\sigma_2}, \tag{B5}$$

$$p_{1z,f} \approx Z\left[\frac{-\sigma z_r}{r_r^2\sqrt{p_{xr}^2\sigma^2+(p_{yr}\sigma+\omega y_r)^2+(p_{zr}\sigma+\omega z_r)^2}}\right]_{\sigma_1}^{\sigma_2}, \tag{B6}$$

with σ_1 and σ_2 being the lower and upper limits of integration, respectively, and $p_{\perp r}=\sqrt{p_{yr}^2+p_{zr}^2}$.

In the rescattering picture, the limits σ_1 and σ_2 can be set to $\pm\infty$, yielding, for fast recollision, Eqs. (23)–(25).

For high-order fast recollision, the recollision picture may break down, which means that the CMT (although being rather small) is not decreasing sharply when the electron leaves the recollision point. In this case, Eqs. (23)–(25) do not provide a good approximation. Our analysis shows that better approximation is achieved with $\sigma_1=-\mathrm{Mod}(u_r,\pi)$ and $\sigma_2=\pi-\mathrm{Mod}(u_r,\pi)$, which correspond to the integration between the surrounding turning points of the trajectory. For fast recollision [i.e., with vanishing laser field $E(u_r)\approx 0$] and beyond the recollision picture, we can set $\sigma_1=-\sigma_2=-\pi/2$ in Eqs. (B4)–(B6), yielding, for fast recollision in the leading term,

$$p_{1x,fb} \approx \frac{2\pi Z p_{\perp r}}{p_{xr}r_r\sqrt{p_r^2\pi^2+4\omega^2 r_r^2}}, \tag{B7}$$

$$p_{1y,fb} \approx -\frac{2\pi Z y_r}{r_r^2\sqrt{p_r^2\pi^2+4\omega^2 r_r^2}}, \tag{B8}$$

$$p_{1z,fb} \approx -\frac{2\pi Z z_r}{r_r^2\sqrt{p_r^2\pi^2+4\omega^2 r_r^2}}. \tag{B9}$$

Let us estimate conditions when the recollision picture is violated. This is the case once the transversal distance at fast recollision is comparable or greater than the amplitude of the quiver motion. There is also a restriction on the longitudinal momentum p_{xr}, which can be derived assuming Eqs. (20) and (21), and (24) and (25), to yield comparable results to rec-CMT. These conditions read

$$r_r \gtrsim \frac{|E(u_r)|}{\omega^2}, \tag{B10}$$

$$p_{xr} \lesssim \sqrt{\frac{|E(u_r)|r_r}{2}}. \tag{B11}$$

APPENDIX C: CALCULATION OF IN-CMT

1. First order in-CMT

The first-order approximation for in-CMT uses the unperturbed trajectory,

$$x_0(\sigma) \approx x_i - \frac{E(u_i)}{2\omega^2}\sigma^2, \tag{C1}$$

$$z_0(\sigma) \approx \frac{p_{\perp i}}{\omega}\sigma, \tag{C2}$$

with the coordinate $z_0(\sigma)$ along the initial transverse momentum, and the momentum corrections in this order are

$$p_{1\parallel}(u) = -\frac{Z}{\omega}\int_{u_i}^{u}\frac{\mathrm{sign}\,[x_0(u)]}{x_0^2(u)}du, \tag{C3}$$

$$p_{1\perp}(u) = -\frac{Z}{\omega}\int_{u_i}^{u}\frac{z_0(u)}{|x_0^3(u)|}du. \tag{C4}$$

The integrals are evaluated for $x_i<0$ as

$$p_{1\parallel}(u) = \frac{Z\sigma}{2x_i^2\omega[1+\sigma^2/\gamma^2(u_i)]}+\frac{Z\gamma(u_i)\arctan\left[\sigma/\gamma(u_i)\right]}{2x_i^2\omega},$$

$$p_{1\perp}(u) = \frac{Zp_{\perp i}}{2E(u_i)x_i^2}\left\{\frac{1}{[1+\sigma^2/\gamma^2(u_i)]^2}-1\right\}, \tag{C5}$$

with $\gamma(u_i)=\sqrt{2I_p}\omega/|E(u_i)|$, which at $\sigma\to\infty$ yields in-CMT formulas as derived in [80], reading

$$p_{1\parallel,\mathrm{in}} = \frac{Z\pi}{\sqrt{2^3|x_i|^3|E(u_i)|}} = \frac{Z\pi E(u_i)}{(2I_p)^{3/2}}, \tag{C6}$$

$$p_{1\perp,\mathrm{in}} = -\frac{Zp_\perp}{2x_i^2|E(u_i)|} = -\frac{2Zp_\perp|E(u_i)|}{(2I_p)^2}. \tag{C7}$$

2. Second-order corrected in-CMT

For calculation of the second-order in-CMT, we need the first-order correction to the trajectory, which is found integrating Eqs. (C5),

$$x_1(\sigma) = \frac{Z\sigma\gamma(u_i)}{2x_i^2\omega^2}\arctan\left[\frac{\sigma}{\gamma(u_i)}\right] \approx \frac{Z\sigma^2}{2\omega^2 x_i^2}, \tag{C8}$$

$$z_1(\sigma) \approx -\frac{Zp_{\perp i}\sigma^3}{6\omega^3|x_i^3|}, \tag{C9}$$

where we keep only the leading terms in the expansion over the small σ. The correction to in-CMT is calculated using the first-order correction to the x coordinate of the trajectory, but neglecting the correction to the z coordinate, as it is small, determined by the small initial transverse momentum.

The second-order corrected in-CMT can be expressed via the exit coordinate x_i,

$$p_{2\parallel,\mathrm{in}} = \frac{\pi Z \,\mathrm{sign}\,[E(u_i)]}{\sqrt{2^3|E(u_i)x_i^3|}}\left[1+\frac{4Z-3p_{\perp i}^2|x_i|}{8|E(u_i)|x_i^2}+O\left(\frac{1}{x_i^4E_0^2}\right)\right], \tag{C10}$$

$$p_{2\perp,\mathrm{in}} = -\frac{Zp_{\perp i}}{2|E(u_i)|x_i^2}\left[1+\frac{4Z-3p_{\perp i}^2|x_i|}{6|E(u_i)|x_i^2}+O\left(\frac{1}{x_i^4E_0^2}\right)\right]. \tag{C11}$$

Let us note that it is easy to identify the term $\sim Z$ in the expansions in Eqs. (C10) and (C11) as the second-order momentum correction, whereas the term $\sim p_{\perp i}^2$ is the correction in the first order due to the transversal motion.

[1] A. M. Perelomov, V. S. Popov, and V. M. Terent'ev, Zh. Exp. Theor. Fiz. **51**, 309 (1966) [Sov. Phys. JETP **24**, 207 (1967)].
[2] A. M. Perelomov and V. S. Popov, Zh. Exp. Theor. Fiz. **52**, 514 (1967) [Sov. Phys. JETP **25**, 336 (1967)].
[3] V. S. Popov, V. P. Kuznetsov, and A. M. Perelomov, Zh. Exp. Theor. Fiz. **53**, 331 (1967) [Sov. Phys. JETP **26**, 222 (1968)].
[4] V. S. Popov, Phys. Usp. **47**, 855 (2004).
[5] V. S. Popov, Phys. Atom. Nuclei **68**, 686 (2005).
[6] S. V. Popruzhenko, J. Phys. B **47**, 204001 (2014).
[7] T. Brabec, M. Y. Ivanov, and P. B. Corkum, Phys. Rev. A **54**, R2551 (1996).
[8] S. P. Goreslavski, G. G. Paulus, S. V. Popruzhenko, and N. I. Shvetsov-Shilovski, Phys. Rev. Lett. **93**, 233002 (2004).
[9] P. B. Corkum, Phys. Rev. Lett. **71**, 1994 (1993).
[10] N. I. Shvetsov-Shilovski, S. P. Goreslavski, S. V. Popruzhenko, and W. Becker, Phys. Rev. A **77**, 063405 (2008).
[11] X. Wang and J. H. Eberly, Phys. Rev. Lett. **103**, 103007 (2009).
[12] X. Wang and J. H. Eberly, Phys. Rev. Lett. **105**, 083001 (2010).
[13] F. Mauger, C. Chandre, and T. Uzer, Phys. Rev. Lett. **104**, 043005 (2010).
[14] C. Liu and K. Z. Hatsagortsyan, Phys. Rev. A **85**, 023413 (2012).
[15] A. Kamor, F. Mauger, C. Chandre, and T. Uzer, Phys. Rev. Lett. **110**, 253002 (2013).
[16] D. Dimitrovski, J. Maurer, H. Stapelfeldt, and L. B. Madsen, Phys. Rev. Lett. **113**, 103005 (2014).
[17] D. Dimitrovski and L. B. Madsen, Phys. Rev. A **91**, 033409 (2015).
[18] J. Maurer, B. Willenberg, J. Daněk, B. W. Mayer, C. R. Phillips, L. Gallmann, M. Klaiber, K. Z. Hatsagortsyan, C. H. Keitel, and U. Keller, Phys. Rev. A **97**, 013404 (2018).
[19] W. Becker, F. Grasbon, R. Kopold, D. B. Milošević, G. G. Paulus, and H. Walther, Adv. Atom. Mol. Opt. Phys. **48**, 35 (2002).
[20] P. Agostini and L. F. DiMauro, Rep. Prog. Phys. **67**, 813 (2004).
[21] M. C. Kohler, T. Pfeifer, K. Z. Hatsagortsyan, and C. H. Keitel, Adv. Atom. Mol. Opt. Phys. **61**, 159 (2012).
[22] W. Becker, X. Liu, P. J. Ho, and J. H. Eberly, Rev. Mod. Phys. **84**, 1011 (2012).
[23] G. L. Yudin and M. Y. Ivanov, Phys. Rev. A **63**, 033404 (2001).
[24] D. Comtois, D. Zeidler, H. Pépin, J. C. Kieffer, D. M. Villeneuve, and P. B. Corkum, J. Phys. B **38**, 1923 (2005).
[25] R. Moshammer, J. Ullrich, B. Feuerstein, D. Fischer, A. Dorn, C. D. Schröter, J. R. Crespo Lopez-Urrutia, C. Hoehr, H. Rottke, C. Trump, M. Wittmann, G. Korn, and W. Sandner, Phys. Rev. Lett. **91**, 113002 (2003).
[26] A. Rudenko, K. Zrost, C. D. Schröter, V. L. B. de Jesus, B. Feuerstein, R. Moshammer, and J. Ullrich, J. Phys. B **37**, L407 (2004).
[27] K. I. Dimitriou, D. G. Arbó, S. Yoshida, E. Persson, and J. Burgdörfer, Phys. Rev. A **70**, 061401 (2004).
[28] A. Rudenko, K. Zrost, T. Ergler, A. B. Voitkiv, B. Najjari, V. L. B. de Jesus, B. Feuerstein, C. D. Schröter, R. Moshammer, and J. Ullrich, J. Phys. B **38**, L191 (2005).
[29] B. Wolter, M. G. Pullen, M. Baudisch, M. Sclafani, M. Hemmer, A. Senftleben, C. D. Schröter, J. Ullrich, R. Moshammer, and J. Biegert, Phys. Rev. X **5**, 021034 (2015).
[30] C. I. Blaga, F. Catoire, P. Colosimo, G. G. Paulus, H. G. Muller, P. Agostini, and L. F. DiMauro, Nat. Phys. **5**, 335 (2009).
[31] F. Catoire, C. Blaga, E. Sistrunk, H. Muller, P. Agostini, and L. DiMauro, Laser Phys. **19**, 1574 (2009).
[32] W. Quan, Z. Lin, M. Wu, H. Kang, H. Liu, X. Liu, J. Chen, J. Liu, X. T. He, S. G. Chen, H. Xiong, L. Guo, H. Xu, Y. Fu, Y. Cheng, and Z. Z. Xu, Phys. Rev. Lett. **103**, 093001 (2009).
[33] C. Y. Wu, Y. D. Yang, Y. Q. Liu, Q. H. Gong, M. Y. Wu, X. Liu, X. L. Hao, W. D. Li, X. T. He, and J. Chen, Phys. Rev. Lett. **109**, 043001 (2012).
[34] B. Wolter, C. Lemell, M. Baudisch, M. G. Pullen, X.-M. Tong, M. Hemmer, A. Senftleben, C. D. Schröter, J. Ullrich, R. Moshammer, J. Biegert, and J. Burgdörfer, Phys. Rev. A **90**, 063424 (2014).
[35] J. Dura, N. Camus, A. Thai, A. Britz, M. Hemmer, M. Baudisch, A. Senftleben, C. D. Schröter, J. Ullrich, R. Moshammer, and J. Biegert, Sci. Rep. **3**, 2675 (2013).
[36] M. G. Pullen, J. Dura, B. Wolter, M. Baudisch, M. Hemmer, N. Camus, A. Senftleben, C. D. Schröter, R. Moshammer, J. Ullrich, and J. Biegert, J. Phys. B **47**, 204010 (2014).
[37] Q. Z. Xia, D. F. Ye, L. B. Fu, X. Y. Han, and J. Liu, Sci. Rep. **5**, 11473 (2015).
[38] K. Zhang, Y. H. Lai, E. Diesen, B. E. Schmidt, C. I. Blaga, J. Xu, T. T. Gorman, F. Légaré, U. Saalmann, P. Agostini, J. M. Rost, and L. F. DiMauro, Phys. Rev. A **93**, 021403 (2016).
[39] E. Diesen, U. Saalmann, M. Richter, M. Kunitski, R. Dörner, and J. M. Rost, Phys. Rev. Lett. **116**, 143006 (2016).
[40] J. B. Williams, U. Saalmann, F. Trinter, M. S. Schöffler, M. Weller, P. Burzynski, C. Goihl, K. Henrichs, C. Janke, B. Griffin, G. Kastirke, J. Neff, M. Pitzer, M. Waitz, Y. Yang, G. Schiwietz, S. Zeller, T. Jahnke, and R. Dörner, J. Phys. B **50**, 034002 (2017).
[41] F. H. M. Faisal, Nat. Phys. **5**, 319 (2009).
[42] C. Liu and K. Z. Hatsagortsyan, Phys. Rev. Lett. **105**, 113003 (2010).
[43] T.-M. Yan, S. V. Popruzhenko, M. J. J. Vrakking, and D. Bauer, Phys. Rev. Lett. **105**, 253002 (2010).
[44] J. Guo, X.-S. Liu, and S.-I. Chu, Phys. Rev. A **82**, 023402 (2010).
[45] C. Liu and K. Z. Hatsagortsyan, J. Phys. B **44**, 095402 (2011).

[46] A. Kästner, U. Saalmann, and J. M. Rost, Phys. Rev. Lett. **108**, 033201 (2012).
[47] C. Lemell, K. I. Dimitriou, X.-M. Tong, S. Nagele, D. V. Kartashov, J. Burgdörfer, and S. Gräfe, Phys. Rev. A **85**, 011403 (2012).
[48] L. Guo, S. S. Han, X. Liu, Y. Cheng, Z. Z. Xu, J. Fan, J. Chen, S. G. Chen, W. Becker, C. I. Blaga, A. D. DiChiara, E. Sistrunk, P. Agostini, and L. F. DiMauro, Phys. Rev. Lett. **110**, 013001 (2013).
[49] S. A. Kelvich, W. Becker, and S. P. Goreslavski, Phys. Rev. A **93**, 033411 (2016).
[50] L. V. Keldysh, Zh. Eksp. Teor. Fiz. **47**, 1945 (1964) [Sov. Phys. JETP **20**, 1307 (1965)].
[51] F. H. M. Faisal, J. Phys. B **6**, L89 (1973).
[52] H. R. Reiss, Phys. Rev. A **22**, 1786 (1980).
[53] S. V. Popruzhenko, G. G. Paulus, and D. Bauer, Phys. Rev. A **77**, 053409 (2008).
[54] S. V. Popruzhenko and D. Bauer, J. Mod. Opt. **55**, 2573 (2008).
[55] L. Torlina and O. Smirnova, Phys. Rev. A **86**, 043408 (2012).
[56] L. Torlina, M. Ivanov, Z. B. Walters, and O. Smirnova, Phys. Rev. A **86**, 043409 (2012).
[57] J. Kaushal and O. Smirnova, Phys. Rev. A **88**, 013421 (2013).
[58] M. Klaiber, E. Yakaboylu, and K. Z. Hatsagortsyan, Phys. Rev. A **87**, 023417 (2013).
[59] M. Klaiber, E. Yakaboylu, and K. Z. Hatsagortsyan, Phys. Rev. A **87**, 023418 (2013).
[60] X.-Y. Lai, C. Poli, H. Schomerus, and C. Figueira de Morisson Faria, Phys. Rev. A **92**, 043407 (2015).
[61] E. Pisanty and M. Ivanov, Phys. Rev. A **93**, 043408 (2016).
[62] T. Keil, S. V. Popruzhenko, and D. Bauer, Phys. Rev. Lett. **117**, 243003 (2016).
[63] D. B. Milošević, Phys. Rev. A **88**, 023417 (2013).
[64] D. B. Milošević, Phys. Rev. A **90**, 063423 (2014).
[65] W. Becker, S. P. Goreslavski, D. B. Milošević, and G. G. Paulus, J. Phys. B **47**, 204022 (2014).
[66] M. Möller, F. Meyer, A. M. Sayler, G. G. Paulus, M. F. Kling, B. E. Schmidt, W. Becker, and D. B. Milošević, Phys. Rev. A **90**, 023412 (2014).
[67] W. Becker and D. B. Milošević, J. Phys. B **48**, 151001 (2015).
[68] J. G. Leopold and I. C. Percival, J. Phys. B **12**, 709 (1979).
[69] B. Hu, J. Liu, and S. Chen, Phys. Lett. A **236**, 533 (1997).
[70] J. S. Cohen, Phys. Rev. A **64**, 043412 (2001).
[71] D. D. Hickstein, P. Ranitovic, S. Witte, X.-M. Tong, Y. Huismans, P. Arpin, X. Zhou, K. E. Keister, C. W. Hogle, B. Zhang, C. Ding, P. Johnsson, N. Toshima, M. J. J. Vrakking, M. M. Murnane, and H. C. Kapteyn, Phys. Rev. Lett. **109**, 073004 (2012).
[72] J. Liu, W. Chen, B. Zhang, J. Zhao, J. Wu, J. Yuan, and Z. Zhao, Phys. Rev. A **90**, 063420 (2014).
[73] A. Ludwig, J. Maurer, B. W. Mayer, C. R. Phillips, L. Gallmann, and U. Keller, Phys. Rev. Lett. **113**, 243001 (2014).
[74] S. Chelkowski, A. D. Bandrauk, and P. B. Corkum, Phys. Rev. A **92**, 051401 (2015).
[75] J. F. Tao, Q. Z. Xia, J. Cai, L. B. Fu, and J. Liu, Phys. Rev. A **95**, 011402 (2017).
[76] T. Keil and D. Bauer, J. Phys. B **50**, 194002 (2017).
[77] A. Di Piazza, C. Müller, K. Z. Hatsagortsyan, and C. H. Keitel, Rev. Mod. Phys. **84**, 1177 (2012).
[78] S. Palaniyappan, I. Ghebregziabher, A. D. DiChiara, J. MacDonald, and B. C. Walker, Phys. Rev. A **74**, 033403 (2006).
[79] M. Klaiber, K. Z. Hatsagortsyan, J. Wu, S. S. Luo, P. Grugan, and B. C. Walker, Phys. Rev. Lett. **118**, 093001 (2017).
[80] N. Shvetsov-Shilovski, S. Goreslavski, S. Popruzhenko, and W. Becker, Laser Phys. **19**, 1550 (2009).
[81] See Supplemental Material at http://link.aps.org/supplemental/10.1103/PhysRevA.97.063409 for the analysis of the precision of the CMT formulas.
[82] I. S. Gradshteyn and I. M. Ryzhik, *Table of Integrals, Series, and Products* (Academic Press, New York, 1965).